

Agitation and mobilization of thixotropic liquids

J.J. Derksen

Chemical & Materials Engineering Department, University of Alberta, Edmonton, Alberta,
T6G 2G6 Canada, jos@ualberta.ca

Submitted to AIChE J, September 2009

Revision submitted: November 2009

Accepted: December 2009

Abstract

Direct numerical simulations of transitional and turbulent flows of purely viscous thixotropic liquids in stirred tanks have been performed. The simple thixotropy model employed is based on the notion of a network in the liquid with an integrity that builds up with finite rate under quiescent conditions and breaks down under liquid deformation. We solve a transport equation for the network integrity which is two-way coupled to the lattice-Boltzmann-based flow solver. The liquid's time scale characterized by the dimensionless Deborah number shows a profound impact on the level of mobilization and the flow patterns in the mixing tanks, especially if the time scale of the liquid is of the same order as the circulation time in the tank. It also is demonstrated to what extent increasing the impeller speed improves mobilization and mixing.

Keywords

thixotropy, direct numerical simulation, lattice-Boltzmann, stirred tank, mixing

Introduction

Processing and handling non-Newtonian liquids is abundant in food, pharmaceutical, paper-and-pulp, and (petro) chemical industries. Process design and process efficiency directly interfere with the liquid's rheological properties since fluid flow and fluid deformation are part of virtually any process step. An interesting and relevant subset of non-Newtonian behavior is thixotropy. Thixotropic liquids show time-dependence, i.e. their constitutive relations contain terms related to the liquid's deformation history. A typical (micro physical/chemical) source of thixotropy is the presence of a structural network in the fluid that forms as a result of long-range interactions between e.g. macro-molecules or microscopic solid particles dispersed in it. A strongly developed network results in a liquid that is hard to deform (highly viscous) and/or has elastic properties. Liquid deformation tends to disintegrate the network. Since usually the rate at which the network disintegrates under deformation, and builds up at quiescent conditions is finite (e.g. due to transport limitations at the micro level), the local deformation history in a Lagrangian frame of reference impacts the local rheological behavior, hence thixotropy.

In many cases agitation of thixotropic liquids in mixing tanks is not so much done to mix the liquid at the molecular or a mesoscopic level; it is in the first place done to mobilize the liquid by breaking the network. The extent to which this happens is an intricate interplay between time scales (of the liquid and of the agitation), liquid inertia (relative to viscous forces), and the geometrical layout of the tank. As an example, we expect interesting hydrodynamics if macroscopic flow time scales such as the period of an impeller revolution, or the liquid's circulation time are of the same order of magnitude as the time scales contained in the liquid's rheological behavior. As in many more situations where interaction and competition of a multitude of phenomena govern process behavior, numerical simulation is a versatile way to reveal the interactions and to gain insight in the relative importance of these phenomena as a function of process conditions. If process conditions are externally controllable, simulations may greatly support process design and optimization.

In this paper a methodology is outlined for direct numerical simulations involving thixotropic liquids agitated in mixing tanks. The numerical efficiency of the methodology allows for fine grids so that transitional and mildly turbulent flows can be fairly accurately resolved. In a recent paper of ours¹ the simulation methodology has been successfully verified by comparing its results with analytical and semi-analytical data of benchmark flows. The focus of the present paper is on the application of the methodology to agitation for mobilizing and mixing thixotropic liquids.

A relatively simple thixotropy model has been adopted. Also, the liquids considered are purely viscous, that is, no visco-elastic effects have been incorporated. In spite of these limitations, the dimensionality of the parameter space is much larger than it would be with simpler (Newtonian) liquids. For this reason we primarily limit our study to three dependencies: the impact of the time scale related to network build-up in the liquid (relative to the flow time scales) on the level of mobilization; the effect of the impeller speed; and the consequences of the agitation geometry. The latter aspect is represented by comparing the performance of two impellers typically used for turbulent agitation of Newtonian liquids, viz. a Rushton turbine and a pitched-blade turbine (PBT).

Literature on turbulent and transitional agitation of non-Newtonian liquids is relatively scarce. It is mostly related to shear-thinning and/or Bingham liquids with a time-independent rheology.²⁻⁶ Stirring yield-stress liquids in mixing tanks usually results in the formation of a cavity around the impeller: liquid only gets agitated in a part of the tank volume around the impeller, and – as for thixotropic liquids – mobilization is a key issue. Recently, agitation of thixotropic liquids was studied experimentally and computationally.⁷ One of the main findings of that study was that the level of realism of simulations would benefit from more refined models for fluid behavior and their computationally efficient implementation in CFD codes. This very well relates to the purpose of the present study.

This paper is organized in the following manner: First the flow geometries are introduced. Then the liquid's rheological model is described. Along with the geometrical characteristics this allows us to define a set of dimensionless numbers that are the coordinates of the parameter space we will be partly

exploring. The subsequent section briefly describes the numerical methodology (more details are in Reference 1). In presenting the results, the focus is on the level of mobilization, and on the flow structures encountered. Next to mobilization also the mixing performance in terms of the time required to mix a passive scalar to a certain level of homogeneity (mixing time) will be discussed. The final section summarizes the results and reiterates conclusions.

Flow geometries

The baffled mixing tanks are filled to a level $H=T$ (with T the tank diameter) with liquid, see Figure 1. A lid closes off the surface, i.e. at the top a no-slip condition applies. Agitation is performed by two different impellers, typically used for turbulent agitation: a Rushton turbine and a pitched-blade turbine (PBT), see Figure 1. The PBT has four blades under an angle of 45° , mounted on a hub. This impeller rotates such that it pumps in the downward direction. The shaft of the PBT runs over the entire tank height. The Rushton turbine has six short, vertical blades mounted on a disk. The disk is mounted on a shaft that enters from the top down to the level of the impeller. The primary flow induced by this impeller is in the radial direction. The Rushton turbine and the PBT both have a diameter equal to $D=T/3$. They rotate with an angular velocity of N revolutions per second.

The choice of these standard impeller and tank configurations allows for relating the present simulations of thixotropic liquid flow with earlier works on Newtonian and also Bingham liquid flow in similar geometries.

Thixotropy model

The thixotropy model we use is based on work that dates back to the late nineteen-fifties.^{8,9} More recently it has been applied by Ferroir et al.¹⁰ in their analysis of particle sedimentation in clay suspensions. It has been placed in a larger context of thixotropy modeling in the review due to Mujumdar et al.¹¹. In the purely viscous (i.e. non-elastic) model we keep track of a scalar λ that varies between 0 and 1 and

indicates the integrity of a structural network in the liquid ($\lambda=0$: no network; $\lambda=1$: fully developed network). Its transport equation reads

$$\frac{\partial \lambda}{\partial t} + u_i \frac{\partial \lambda}{\partial x_i} = -k_1 \dot{\gamma} \lambda + k_2 (1 - \lambda) \quad (1)$$

(summation over repeated indices) with u_i the i^{th} component of the fluid velocity vector, and

$\dot{\gamma} = \sqrt{2d_{ij}d_{ij}}$ a generalized deformation rate; $d_{ij} = \frac{1}{2} \left(\frac{\partial u_j}{\partial x_i} + \frac{\partial u_i}{\partial x_j} \right)$ is the rate of strain tensor. The first term

on the right hand side of Eq. 1 indicates breakdown of the network due to liquid deformation; the second

term is responsible for build-up of the network with a time constant $\frac{1}{k_2}$ associated to it. The network

integrity is fed back to the liquid flow by relating it to the apparent viscosity η_a . The simple model¹⁰ used

here adopts a linear relation:

$$\eta_a = \eta_\infty (1 + \alpha \lambda) \quad (2)$$

In a homogeneous shear field with shear rate $\dot{\gamma}$, the steady-state solution to Eq. 1 reads

$$\lambda_{ss} = \frac{k_2}{k_1 \dot{\gamma} + k_2} \quad (3)$$

The associated steady state viscosity is (combine Eqs. 2 and 3)

$$\eta_{ss} = \eta_\infty \left(1 + \alpha \frac{k_2}{k_1 \dot{\gamma} + k_2} \right) \quad (4)$$

The parameter η_∞ can thus be interpreted as the infinite shear viscosity. The zero-shear viscosity is

$\eta_\infty (1 + \alpha)$. A typical representation of the steady-state rheology (Eq. 4) is given in Figure 2.

The thixotropic liquid as defined by Eqs. 1 and 2 has four parameters: $k_1, k_2, \eta_\infty, \alpha$. This implies that once the flow geometry is defined, four dimensionless numbers are needed to fully pin down the flow conditions. Three of the dimensionless numbers are quite straightforward: (1) a Reynolds number defined

in the same way as traditionally done in Newtonian stirred tank flow but now with η_∞ : $Re_\infty = \frac{\rho ND^2}{\eta_\infty}$;

(2) the ratio of zero-shear over infinite-shear viscosity $\alpha+1$; and (3) a time-scale ratio that we term

Deborah number: $Db = \frac{N}{k_2}$ (having a Deborah number does not mean we consider visco-elasticity). Db is

the ratio of the time scale of the liquid divided by a macroscopic flow time scale for which we take the

period of one impeller revolution ($\frac{1}{N}$). The choice of the fourth dimensionless number relates to the

application perspective. If the rheogram in Figure 2 is interpreted as that of a (pseudo) Bingham liquid the

intercept of the asymptote for high shear rates with the ordinate can be viewed as a pseudo yield stress:

$\tau_Y = \eta_\infty \alpha \frac{k_2}{k_1}$ (see Figure 2). The fourth dimensionless number then becomes a pseudo-Bingham number:

$Bn = \frac{\tau_Y}{\eta_\infty N} = \alpha \frac{k_2}{k_1} \frac{1}{N}$. However, if the liquid is merely interpreted as shear thinning, the ratio $\frac{k_2}{k_1}$ can be

viewed as the liquid's "characteristic" shear rate $\dot{\gamma}_c$ (characteristic in the sense that the transition from

zero-shear to infinite-shear viscosity takes place around $\dot{\gamma} = \dot{\gamma}_c$, see Eq. 4) and the dimensionless number

would be typically chosen as $\frac{\dot{\gamma}_c}{N}$. In this paper the Bingham liquid perspective will be taken, and the

pseudo-Bingham number will be used so that the four dimensionless numbers are Re_∞ , α , Db , and Bn .

Numerical approach

The lattice-Boltzmann method (LBM) has been applied to numerically solve the incompressible flow equations. The method originates from the lattice-gas automaton concept as conceived by Frisch,

Hasslacher, and Pomeau in 1986.¹² Lattice gases and lattice-Boltzmann fluids can be viewed as

(fictitious) fluid particles moving over a regular lattice, and interacting with one another at lattice sites.

These interactions (collisions) give rise to viscous behavior of the fluid, just as colliding/interacting

molecules do in real fluids. Since 1987 particle-based methods for mimicking fluid flow have evolved

strongly, as can be witnessed from review articles and text books.¹³⁻¹⁶ More recently also applications of the LBM in non-Newtonian fluid mechanics have been reported (e.g. References 6,17,18). The main reasons for employing the LBM for fluid flow simulations are its computational efficiency and its inherent parallelism, both not being hampered by geometrical complexity.

In this paper the LBM formulation of Somers¹⁹ has been employed. It falls in the category of three-dimensional, 18 speed (D3Q18) models. Its grid is uniform and cubic. Planar, no-slip walls naturally follow when applying the bounce-back condition. For non-planar and/or moving walls (that we have in case we are simulating the flow in a cylindrical, baffled mixing tank with a revolving impeller) an adaptive force field technique (a.k.a. immersed boundary method) has been used.^{20,21}

To incorporate thixotropy, the viscosity needs to be made dependent on the local value of the network parameter λ (Eq. 2), and (more importantly) the transport equation for the network parameter (Eq. 1) needs to be solved. We solve Eq. 1 with an explicit finite volume discretization on the same (uniform and cubic) grid as the LBM. A clear advantage of employing a finite volume formulation is the availability of methods for suppressing numerical diffusion. This is particularly important in the present application since Eq. 1 does not have a molecular or turbulent diffusion term; in order to correctly solve Eq. 1 we cannot afford to have significant numerical diffusion. As in previous works^{22,23}, TVD discretization with the Superbee flux limiter for the convective fluxes²⁴ was employed. We step in time according to an Euler explicit scheme. This finite volume formulation for scalar transport does not hamper the parallelism of the overall numerical approach.

The presence of a source term (i.e. the right-hand side) in Eq. 1, combined with the explicit nature of the time stepping in some (rare) cases (specifically related to large k_2 , i.e. quickly responding liquids) gives rise to unstable behavior. This can be effectively countered by treating the right-hand side semi-implicitly, i.e. by evaluating it for λ at the new time level. In that case the discrete version of Eq. 1 schematically reads

$$\frac{\lambda^{(n+1)} - \lambda^{(n)}}{\Delta t} + \left(u_i \frac{\partial \lambda}{\partial x_i} \right)^{(n)} = -k_1 \dot{\gamma}^{(n)} \lambda^{(n+1)} + k_2 (1 - \lambda^{(n+1)}) \quad (6)$$

with the upper index indicating the (discrete) time level. Equation 6 can be rewritten as an explicit expression in $\lambda^{(n+1)}$ since no spatial derivatives are evaluated at the new time level. In an earlier paper ¹ we have shown that for situations where an explicit formulation is stable, an implicit treatment of the source term results only in insignificant differences with explicit results.

Physical, dimensionless and numerical settings

The values for the infinite-shear viscosity η_∞ and the zero-shear viscosity $\eta_\infty(1+\alpha)$ were chosen such that the flow in the mixing tanks would be mildly turbulent if the liquid would be Newtonian with viscosity η_∞ (Re_∞ of the order of 10^4), and laminar with viscosity $\eta_\infty(1+\alpha)$ ($\frac{\text{Re}_\infty}{1+\alpha} = O(10^2)$). With the lattice-Boltzmann flow solver (that enables the use of fine grids) in place, these Reynolds numbers allow for direct numerical simulations (DNS). This way we avoid the use of turbulence closure relations or subgrid-scale modelling. With DNS we fully resolve the (likely complex) interactions between liquid properties and flow structures, without having to consider potential artefacts related to turbulence modelling. Also, the state-of-the-art of turbulence modelling of non-Newtonian liquid flow is not as strongly developed as that of flow of Newtonian liquids.

The tanks to be simulated are of lab-scale size with a tank volume of typically 10 liter. 10 liter tanks with geometrical layouts as given in Figure 1 have a diameter $T=0.234$ m. The impeller diameter $D=T/3=0.078$ m. With a liquid having $\eta_\infty = 10^{-2}$ Pa·s and $\rho=10^3$ kg/m³ we generate mildly turbulent flow if the impeller spins with $N=10$ rev/s: $\text{Re}_\infty=6 \cdot 10^3$. Commonly used thixotropic liquids have time constants in the range of 0.1 to 10 s (see e.g. Dullaert & Mewis ²⁵), so that the Deborah numbers fall in the range 1 to 100.

In this paper we only explore part of the four-dimensional parameter space as defined by the four dimensionless numbers Re_∞ , Db , Bn , and $\alpha+1$. The viscosity ratio $\alpha+1$ has been set to a fixed value of 100. This way we ensure laminar flow if the network would be fully developed ($\lambda=1$ everywhere). Three Deborah numbers will be considered: 1, 10, and 100. In addition, cases will be discussed where the liquid has a time-independent, shear thinning rheology according to Eq. 4. Effectively this implies that the liquid adapts infinitely fast so that $\frac{1}{k_2} \rightarrow 0$ and $Db=0$. For these four Db numbers, the base-case impeller speed has been chosen such that $Re_\infty=6 \cdot 10^3$, and $Bn=100$. Under these conditions (tank size, impeller speed, other liquid properties) $Bn=100$ corresponds to a (pseudo) yield stress of $\tau_Y=10 \text{ N/m}^2$ which is a typical yield stress for a clay suspension. As we will see, under these base-case conditions the liquid sometimes gets only partially (and sometimes only marginally) mobilized. In order to check to what extent increasing the impeller speed helps in mobilizing the liquid also higher impeller speeds are investigated. At higher impeller speeds Re_∞ and Db increase, while Bn decreases.

In its basic implementation (as used in this study) the lattice-Boltzmann method applies a uniform, cubic grid. The spatial resolution of the grid was such that the tank diameter T equals 180 grid spacings Δ ($\Delta=T/180$). The time step is such that the impellers revolves once in 2000 time steps. The rotation of the impeller in the static grid is represented by an immersed boundary technique. In order to assess grid effects, two flow cases were also simulated on a grid with resolution $\Delta=T/240$, and compared with their $T/180$ counterparts in terms of global characteristics as well as the spatial distribution of the structure parameter λ in the stirred tank.

As the default situation, the simulations were started with a zero liquid velocity field and a uniform network parameter $\lambda=1$ (fully developed network). This mimics the common situation that the liquid has been standing still for sufficient time to develop a network after which we turn on the agitation to mobilize it. In a few cases we also started spinning the impellers from a liquid without a network ($\lambda=0$ throughout the tank). Our primary interests are in how the flow develops towards a (quasi) steady state,

what flow structures can be observed in (quasi) steady state, and what the influence of the Deborah number and the impeller speed is on all this.

Results

Flow evolution from startup

In order to assess how the flow in the tank evolves from a zero-velocity, fully networked ($\lambda = 1$) state towards a quasi steady, agitated state we show in Figure 3 time series of the tank-averaged network parameter $\langle \lambda \rangle$ for $Db=10$ (and further base-case conditions, $Re_\infty = 6 \cdot 10^3$, $Bn=100$, $\alpha+1=100$) for the two impellers considered. Obviously agitation breaks down the network to a large extent. At $Db=10$, it does so on a time scale of a few tens of impeller revolutions, with differences between the two impellers. In fact, the route towards steady state with the Rushton turbine is quite peculiar. After some 40 revolutions - when it looks like a steady state with $\langle \lambda \rangle \approx 0.33$ has been established - $\langle \lambda \rangle$ starts increasing slightly, however significantly with a final steady state that has $\langle \lambda \rangle \approx 0.39$ reached after about 100 impeller revolutions. At the same Deborah number the flow generated by the PBT goes seemingly to a steady state via a simpler decay process that takes approximately 40 revolutions.

In order to interpret the evolution of the mobilization process at $Db=10$ in more detail, scalar distributions in the vertical, mid-baffle plane at various stages are given in Figure 4. The Rushton turbine first reduces the network parameter in its direct vicinity after which the breakdown process spreads throughout the tank. The slight increase of $\langle \lambda \rangle$ that sets in after 40 impeller revolutions as observed in Figure 3 is due to an intricate interplay between macro-scale flow and thixotropy effects. The strong radial stream emerging from the impeller and hitting the tank wall starts deflecting more and more downwards, thereby favoring the strength of the flow in the lower part of the tank, and weakening the flow in the upper part of the tank. This is a positive feedback process: It allows the network in the upper part of the tank to recover which further contributes to the downward deflection of the impeller stream

and weakening the flow in the upper part even further. After roughly 100 revolutions the flow has settled in a state with strong flow in the volume below the impeller, and weak flow (and marginal mobilization) in the volume above.

At $Db=10$ also the flow generated by the PBT goes through interesting transitional stages (Figure 4, bottom panels), very much different from the flow generated by the Rushton turbine though. Initially the stream emerging from this axially pumping impeller gets deflected radially and hits the tank wall at approximately at $z=0.2T$ in a (left-right in Figure 4) symmetric pattern. After approximately 80 impeller revolutions this pattern gets unstable, and left-right symmetry is broken. Now from time to time the impeller stream reaches much lower vertical locations and then gets pushed up again allowing the stream at the other side to reach lower in a quasi periodic manner. To illustrate this unstable behaviour we show (in Figure 5) a time series of λ in a point in the lower-left corner of the plane shown in Figure 4. After a quick decline of λ (first 20 revolutions, see Figure 5) the flow goes through a stage with slow development of the local network parameter (between 20 and 80 revolutions) after which the quasi periodic behaviour sets in with a period time of the order of 5 impeller revolutions.

The Deborah number (and thus the time-dependent nature of the liquids) appears to be a crucial parameter for the level of mobilization and (related) flow structures in the tank. In Figure 6 we show how much differently $\langle \lambda \rangle$ evolves in the mixing tanks if $Db=1, 10, \text{ or } 100$. It is worthwhile noting that under steady, homogeneous shear conditions the three liquids as used in Figure 6 display exactly the same shear-thinning behaviour (according to Eq. 4).

The lower the Deborah number, the faster the flow reaches (quasi) steady state, and also the higher the steady-state $\langle \lambda \rangle$. For low Deborah numbers, the liquid responds quickly to deformation (and absence of deformation). Therefore the regions in the liquid undergoing strong deformation due to agitation (notably the impeller-swept volume, and the impeller stream) largely overlap with regions of low λ . Given the liquid's quick response, the low- λ regions do not get a chance to be transported to the rest of the tank, leaving that part quite inactive (similar to cavern formation with Bingham liquids) and giving

rise to relatively high tank-averaged network parameters. As we discussed above, the interactions between liquid and flow time scales give rise to a complex evolution of the flow for $Db=10$. If Db increases further to 100, the delay between the moment the deformation is applied to the liquid and the destruction of the network increases, so that high deformation regions get dislocated from low viscosity regions. Similarly, more quiescent regions not necessarily get the change to develop high apparent viscosities. At $Db=100$ the liquid is responding so slow that the network parameter λ gets fairly uniformly distributed in the tank (in a way this is analogous with very slow chemical reactions occurring in turbulent flow; if the time scales of the reactions are large compared to the flow time scales, chemical species concentrations tend to uniformity allowing the use of ideally mixed CSTR concepts).

In Figure 7 we show typical distributions of λ after quasi-steady state has been reached for $Db=0$, 1, and 100. For $Db=0$, the transport equation in λ (Eq. 1) does not need to be solved; it can be determined directly from the local $\dot{\gamma}$ and Eq. 3. Comparison of infinitely fast liquids ($Db=0$) and time-dependent liquids agitated such that $Db=1$ shows minor differences. This implies that the liquid's time dependence plays a minor role if it is agitated at $Db=1$. At the other side of the spectrum, for large Db ($Db=100$), λ gets (more or less) uniformly distributed throughout the tank. For the specific cases considered here we expect laminar flow; the uniformity of λ results in a uniform and relatively high viscosity: for the Rushton turbine in quasi steady state $\langle\lambda\rangle\approx 0.30$ so that $\langle\eta_a\rangle\approx 30\eta_\infty$ and

$\langle Re\rangle = \frac{\rho ND^2}{\langle\eta_a\rangle} \approx 200$; for the pitched blade turbine the network is on average a bit more developed

resulting in $\langle Re\rangle = \frac{\rho ND^2}{\langle\eta_a\rangle} \approx 150$.

For the λ -fields depicted in Figure 7 at $Db=1$ and $Db=100$, the corresponding velocity vector plots are given in Figure 8. For the pitched-blade turbine at $Db=1$ the impeller stream is transitional / turbulent whereas the liquid in the upper half of the tank is virtually immobile. As expected, at $Db=100$ the flow is laminar, however with a better overall mobility compared to the $Db=1$ case. Compared to the pitched-

blade turbine, the radial stream being redirected up and down at the tank wall generated by the Rushton turbine helps in mobilization at $Db=1$. At $Db=100$ the two impellers perform similarly in terms of liquid agitation.

An obvious way of enhancing liquid mobility is increasing the impeller speed N . Since changing N has consequences for three of the four dimensionless numbers that have been identified above we have chosen to present the simulation results directly as a function of the impeller speed relative to the base-case impeller speed (that gave rise to $Re_\infty = 6 \cdot 10^3$, $Bn=100$): Figure 9 shows the impact of impeller speed on the eventual (steady-state) tank-averaged network parameter $\overline{\langle \lambda \rangle}$ (averaging over tank volume and time). The different liquids have been identified by their Deborah numbers under base case impeller speed (denoted Db -base in Figure 9). The network breaks down to an increasing extent with an increase of the impeller speed; approximately in an exponential manner (the dashed trend line in Figure 9 represents $\overline{\langle \lambda \rangle} = 10^{-\beta \frac{N}{N_{base}}}$ with $\beta = 0.43$).

Slower liquids (liquids with higher Db -base values) benefit relatively more from increasing the impeller speed than faster liquids, especially in terms of the enhanced agitation mobilizing bigger parts of the tank. This is illustrated for two pitched-blade turbine cases in Figure 10. This figure shows velocity vectors at an impeller speed that is three times higher than the vector fields of Figure 8 (for the rest the conditions are the same). Figure 10 indicates more active volume for Db -base=100 compared to Db -base=1. The λ contour plots (Figure 11) confirm this with lower network parameters in the upper part of the tank for higher Db -base. The Rushton turbine cases show a qualitatively similar trend (not shown for brevity).

All simulations so far were at a spatial resolution such that the tank diameter is spanned by 180 lattice spacings: $\Delta=T/180$. In order to assess grid effects, two Rushton turbine flow cases that we did with $\Delta=T/180$ were repeated with $\Delta=T/240$. For the latter we used a parallel implementation of the computer code; usually running on 6 cpu's in parallel. If we compare the evolution of the tank-average structure

parameter $\langle \lambda \rangle$, the simulations at the two resolutions agree very well, see Figure 12. Looking into more detail reveals some deviation though: in Figure 13 time-averaged, impeller-angle-resolved structure parameters over a vertical cross section are shown. The case with higher spatial resolution shows slightly better mobilization (lower λ) in the upper parts of the tank volume. Generally speaking, however, the results with different resolution agree reasonably well.

Passive scalar transport

Next to mobilization, also mixing is at issue when agitating thixotropic liquids. To quantify mixing, in a few of the simulations discussed above a passive scalar has been tracked during the start-up and quasi-steady-state stages the simulations are going through. We specifically study the base-case flow generated with a PBT at $Db=10$, and the same case with a three times higher impeller speed. For reference also a Newtonian system with the base-case Reynolds number ($Re=6000$) has been simulated.

The default initial conditions for the velocity and network integrity apply (zero flow, fully developed network). As the initial condition for the passive scalar we set its concentration to $c = 1$ in the upper half of the tank ($z \geq \frac{H}{2}$, z defined in Figure 1), and $c = 0$ in the rest of the tank. For c we solve a

convection-diffusion equation: $\frac{\partial c}{\partial t} + u_i \frac{\partial c}{\partial x_i} = \Gamma \frac{\partial^2 c}{\partial x_i^2}$. The numerical method used for solving the passive

scalar concentration field is the same as used for solving λ , i.e. TVD discretization and Euler forward time stepping with the same (uniform cubic) grid as used for λ . In the computer code, the diffusivity has been set to $\Gamma = 10^{-3} \frac{\eta_\infty}{\rho}$. In turbulent flow such a low value makes the microscopic scalar scales much

smaller than the microscopic turbulence scales and full resolution of the micro scalar scales is generally not achieved. In the simulations – specifically those with strong turbulence - the effective diffusivity is largely determined by the grid resolution. However, the simulated concentration fields (reflecting a low-

passed filtered version of the actual fields) serve the purpose of quantifying the macroscopic transport of the passive scalar.

Passive scalar concentrations in a vertical field, midway between baffles are shown in Figure 14. At $Re=6000$ the Newtonian liquid is clearly turbulently agitated. At $tN=20$, the scalar field still remembers its initial status with high concentration in the top part, and low concentration at the bottom; at $tN=40$ the tank's content is largely mixed with, however, still some high concentration spots at the top surface. Compared with this, the base-case with $Db=10$ (and $Re_\infty = 6000$, $Bn=100$, $\alpha+1=100$) gets poorly mixed. The limited liquid mobilization of the top of the tank as witnessed in Figure 4 translates in concentrations remaining close to $c=1$ for at least 40 impeller revolutions. The coherence of structures and left-right symmetry in Figure 14 (middle panels) indicates laminar flow. Increasing the impeller speed by a factor of three turns the flow into a turbulent one and enables mobilization and mixing throughout the tank (Figure 14, bottom panels).

The observations in Figure 14 are quantified and monitored over longer periods of time by means of the normalized standard deviation σ of the concentration in a vertical, mid-baffle plane through the center of the tank. The standard deviation as a function of time is based on vertical snapshots of the passive scalar field like the ones presented in Figure 14: $\sigma^2(t) = \frac{1}{c_{av}^2(t)A} \iint (c^2(\mathbf{x},t) - c_{av}^2(t)) dA$ with A the plane's surface area and $c_{av}(t) = \frac{1}{A} \iint c(\mathbf{x},t) dA$ the plane-averaged concentration. Figure 15 shows the σ time series and reflect the observations made in Figure 14. By 74 impeller revolutions, the standard deviation for the Newtonian case has reduced by two orders of magnitude. The base-case with $Db=10$ only reaches down to a level of $\sigma=0.21$ after 120 impeller revolutions and appears to be leveling off at that stage. Increasing the impeller speed by a factor of three helps in bringing down the passive scalar standard deviation; it gets to a level of 0.032 after 120 impeller revolutions.

Summary & outlook

In this paper, a procedure for detailed simulations of flow of thixotropic liquids is applied to transitional and mildly turbulent agitated tank flow. Thixotropy is considered to be the result of the finite rate response of the integrity of a network in the liquid to local flow conditions. The thixotropy model used is very simple: It is purely viscous, it assumes linear relations for network build-up and breakdown (the latter due to deformation), and a linear relation between apparent viscosity and network integrity. This simple model, however, already comes with four parameters. Where single-phase mixing tank flow of Newtonian liquids can be captured by a single dimensionless number – the Reynolds number – (once the tank and impeller geometry in terms of aspect ratios has been defined, and if the tank does not have a free surface), we now need four dimensionless numbers to pin down the flow conditions. In this paper these dimensionless numbers are a Reynolds number Re_∞ based on the infinite-shear viscosity, a Deborah number Db being the time scale of the liquid relative to the time of a single impeller revolution, a pseudo-Bingham number Bn , and the ratio of zero-shear over infinite-shear viscosity. The aim of this paper is to see how thixotropy qualitatively impacts global flow structures and mixing and liquid mobilization in agitated tanks. For this we explore part of the dimensionless parameter space and consider two different agitation devices, viz. a tank agitated by a Rushton turbine and one by a pitched-blade turbine. Exploring the full parameter space is unpractical given its four-dimensionality combined with the significant computational effort per simulation. In our base-case simulations we fix the Reynolds number to $Re_\infty = 6 \cdot 10^3$ which allows us to perform DNS, the Bingham number to $Bn=100$ which translates to a pseudo yield stress of order 10 N/m^2 in our lab-scale (10 liter) setups, and the viscosity ratio to 100.

The primary characteristic of thixotropy is the effect of the deformation history on the liquid's rheological behavior. In terms of the dimensionless numbers considered here, thixotropic liquids give rise to non-zero Deborah number. For this reason we studied the effect the Deborah number has on the flow. Comparing flows with $Db=1$ and $Db=0$ only shows marginal differences which implies that the liquid's time dependence is not strongly felt if its time scale is of the order of the time required for one impeller revolution. At $Db=100$, i.e. at the other side of the Db -range considered, a slow evolutions towards a

fairly homogeneous distribution of the network parameter is observed resulting in – given the rest of the conditions – laminar flow. The uniformity is due to the large delay between deformation and network breakdown, and the slow build-up of the network under quiescent conditions. The more intriguing situations occur when $Db=10$. These cases show the strongest interaction between flow and liquid time scale, the reason probably being that the liquid time scale now gets comparable to the circulation time of the liquid in the tank (the flow numbers for the Rushton turbine and PBT are roughly equal to one which results in a circulation time of approximately $20/N$, see e.g. Reference 26). The Rushton turbine flow at $Db=10$ slowly (over some 100 revolutions) evolves to the undesired situation with strong flow underneath the impeller, and a largely immobile volume above. The flow generated by the PBT develops a coherent instability with a frequency of $0.2N$.

Given the sometimes poorly mobilized tank volumes we subsequently studied to what extent increasing the impeller speed improves overall mobilization (the latter is characterized by the steady-state, volume averaged network integrity parameter $\overline{\langle \lambda \rangle}$). It does so in a fairly universal manner, i.e. quite independent of the base-case Deborah number or impeller type; tentatively according to an exponential

function: $\overline{\langle \lambda \rangle} = 10^{-\beta \frac{N}{N_{base}}}$ with $\beta = 0.43$.

Passive scalar mixing is largely slaved to the levels of liquid mobilization achieved by the impeller. As shown for a few cases, limited mobilization keeps parts of the tank volume unmixed for long times. Again the effect of increasing the impeller speed has been studied.

The results presented in this paper are largely qualitative, and sensitive to the specific thixotropy model chosen. However, they do show the rich response of stirred tank flow to thixotropy. Furthermore, the methodology as outlined here is generic and can be easily adapted to more complicated (albeit viscous) rheological liquid descriptions. The method is computationally efficient (as demonstrated by the significant number of flow systems, and the significant numbers of impeller revolutions per flow system simulated) and geometrically flexible so that attacking practical mixing and mobilization problems is

within reach. By means of parallelization the spatial resolution can be easily enhanced. This helps in extending the range of Reynolds numbers for which DNS can be performed.

References

- [1] Derksen JJ, Prashant. Simulations of complex flow of thixotropic liquids. *J Non-Newtonian Fluid Mech.* 2009; 160: 65-75.
- [2] Elson TP, Cheesman DJ, Nienow AW. X-ray studies of cavern sizes and mixing performance with fluids possessing a yield stress. *Chem. Engng Sci.* 1986; 41: 2555-2562.
- [3] Elson TP. The growth of caverns formed around rotating impellers during the mixing of a yield stress fluid. *Chem Eng Commun.* 1990; 41:2555-2562.
- [4] Amanullah A, Hjorth SA, Nienow AW. A new mathematical model to predict cavern diameters in highly shear thinning, power law liquids using axial flow impellers. *Chem Engng Sc.* 1998; 53: 455-469.
- [5] Arratia PE, Kukura J, Lacombe J, Muzzio FJ. Mixing of shear-thinning fluids with yield stress in stirred tanks. *AIChE J.* 2006; 52: 2310-2322.
- [6] Derksen JJ. Solid particle mobility in agitated Bingham liquids. *Ind Eng Chem Res.* 2009; 48: 2266-2274.
- [7] Couerbea G, Fletcher DF, Xuereb C, Poux M. Impact of thixotropy on flow patterns induced in a stirred tank: Numerical and experimental studies. *Chem Engng Res Des.* 2008; 86: 545–553.
- [8] Storey BT, Merrill EW. The rheology of aqueous solution of amylose and amylopectine with reference to molecular configuration and intermolecular association. *J Polym Sci.* 1958; 33: 361-375.
- [9] Moore F. The rheology of ceramic slips and bodies. *Trans Br Ceramic Soc.* 1959; 58: 470-494.
- [10] Ferroir T, Huynh HT, Chateau X, Coussot P. Motion of a solid object through a pasty (thixotropic) fluid. *Phys Fluids.* 2004; 16: 594-601.
- [11] Mujumdar A, Beris AN, Metzner AB. Transient phenomena in thixotropic systems. *J Non-Newtonian Fluid Mech.* 2002; 102: 157-178.

- [12] Frisch U, Hasslacher B, Pomeau Y. Lattice-gas automata for the Navier-Stokes Equation. *Phys Rev Lett*. 1986; 56: 1505-1508.
- [13] Chen S, Doolen GD. Lattice Boltzmann method for fluid flows. *Annu Rev Fluid Mech*. 1989; 30: 329-364.
- [14] Yu DZ, Mei RW, Luo LS, Shyy W. Viscous flow computations with the method of lattice Boltzmann equation. *Progr Aerosp Sci*. 2003; 39: 329-367.
- [15] Succi S. *The lattice Boltzmann equation for fluid dynamics and beyond*. Oxford: Clarendon Press; 2001.
- [16] Sukop MC, Thorne DT Jr. *Lattice Boltzmann Modeling: An Introduction for Geoscientists and Engineers*. Berlin: Springer; 2006.
- [17] Yoshino M, Hotta Y, Hirozane T, Endo M. A numerical method for incompressible non-Newtonian fluid flows based on the lattice Boltzmann method. *J Non-Newtonian Fluid Mech*. 2007; 147: 69-78.
- [18] Vikhansky A. Lattice-Boltzmann method for yield-stress liquids. *J Non-Newtonian Fluid Mech*. 2008; 155: 95-100.
- [19] Somers JA. Direct simulation of fluid flow with cellular automata and the lattice-Boltzmann equation. *Appl Sci Res*. 1993; 51: 127-133.
- [20] Goldstein D, Handler R, Sirovich L. Modeling a no-slip flow boundary with an external force field. *J Comp Phys*. 1993; 105: 354-366.
- [21] Derksen J, Van den Akker HEA. Large-eddy simulations on the flow driven by a Rushton turbine. *AIChE J*. 1999; 45: 209-221.
- [22] Hartmann H, Derksen JJ, Van den Akker HEA. Mixing times in a turbulent stirred tank by means of LES. *AIChE J*. 2006; 52: 3696-3706.
- [23] Derksen JJ. Scalar mixing by granular particles. *AIChE J*. 2008; 54: 1741-1747.

- [24] Sweby PK. High resolution schemes using flux limiters for hyperbolic conservation laws. *SIAM J Numer Anal.* 1984; 21: 995-1011.
- [25] Dullaert K, Mewis J. Thixotropy: Build-up and breakdown curves during flow. *J Rheol.* 2005; 49: 1213-1230.
- [26] Tiljander P, Ronnmark B, Theliander H. Characterisation of three different impellers using the LDV-technique. *Can J Chem Engng.* 97; 75: 787-793.

Figure captions

Figure 1. The two stirred tank geometries considered in this paper. Top: baffled tank with Rushton turbine (left: side view, right: top view); bottom: baffled tank with pitched-blade impeller. The (r,z) coordinate system has its origins in the center at the bottom of the tank.

Figure 2. Steady-state rheology according to Eq. 4. The infinite-shear viscosity is η_∞ , the zero-shear viscosity is $\eta_\infty(1+\alpha)$. The pseudo yield stress τ_y is defined by extrapolating the infinite shear behavior towards $\dot{\gamma}=0$.

Figure 3. Time series of the tank average network parameter $\langle\lambda\rangle$ for $Db=10$, starting at $t=0$ from a zero flow field and $\lambda=1$ everywhere. Solid line: pitched blade turbine; dashed line: Rushton turbine.

Figure 4. Instantaneous realizations of the λ -field in the vertical plane midway between baffles. Base-cases with $Db=10$. Top row: Rushton turbine flow at (from left to right) 10, 40, 70, 100, and 180 impeller revolutions after start-up; bottom row: pitched blade turbine flow after 10, 30, 90, 93, and 95 impeller revolutions.

Figure 5. Time series of λ at the point $\frac{2r}{T}=0.91, \frac{z}{T}=0.056$ in the mid-baffle plane for the PBT case with $Db=10$.

Figure 6. Time series of the tank average network parameter $\langle\lambda\rangle$ for three Deborah numbers as indicated. Top panel: pitched-blade turbine; bottom panel: Rushton turbine.

Figure 7. Instantaneous realizations of the λ -field in the vertical plane midway between baffles after quasi steady-state has been reached. Top row: pitched blade turbine flow with (from left to right) $Db=0, 1, \text{ and } 100$. Bottom row: Rushton turbine flow with (from left to right) $Db=0, 1, \text{ and } 100$.

Figure 8. Snapshot of velocity vectors in the mid-baffle plane in the tank equipped with a pitched blade turbine for $Db=1$ (top-left) and $Db=100$ (top-right), and with a Rushton turbine for $Db=1$ (bottom-left) and $Db=100$ (bottom-right) after quasi steady state has been reached.

Figure 9. Time and tank-average network parameter $\overline{\langle\lambda\rangle}$ as a function of impeller speed relative to the base-case impeller speed. Time averaging was performed after (quasi) steady state was reached. The dashed line illustrates the general trend.

Figure 10. Snapshot of velocity vectors in a vertical, mid-baffle plane. Pitched-blade turbine flow with $Db\text{-base}=1$ (left), and $Db\text{-base}=100$ (right), and three times the impeller speed as the base-case.

Figure 11. Snapshots of λ -contours for three times the base-case impeller speed. Pitched-blade turbine flow with (from left to right) $Db\text{-base}=1, 10, 100$ respectively. Note the small high- λ spots in the upper corners of the right panel.

Figure 12. Time series of tank average structure $\langle\lambda\rangle$ parameter for simulations with different spatial resolution. Dashed curves: $\Delta = \frac{T}{180}$; solid curves: $\Delta = \frac{T}{240}$. Top: $Re=6000, Db=1$ starting from a zero

flow field and $\lambda = 0$ everywhere. Bottom: $Re=18000$, $Db=30$ ($Db\text{-base}=10$) starting from a zero flow field with $\lambda = 1$ everywhere. Rushton turbine.

Figure 13. Averaged λ -contours in the vertical, mid-baffle plane for Rushton turbine simulations. These are impeller-angle resolved averages, i.e. the averages are conditioned with the impeller angle. In the panels shown the condition is such that an impeller blade is in the mid-baffle plane. Top row: $Re=6000$, $Db=1$; left resolution such that $\Delta = \frac{T}{180}$, right $\Delta = \frac{T}{240}$. Bottom row: $Re=18000$, $Db=30$ ($Db\text{-base}=10$); left resolution such that $\Delta = \frac{T}{180}$, right $\Delta = \frac{T}{240}$.

Figure 14. Instantaneous passive scalar concentrations in vertical mid-baffle planes. Left panels: 20 revolutions after start up; right panels: 40 revolutions after start up. Top: Newtonian liquid agitated at $Re=6000$; middle: base-case with $Db=10$; bottom: $Db\text{-base}=10$ with a 3 times higher impeller speed.

Figure 15. Time series of the passive scalar standard deviation σ in the vertical, mid-baffle plane. Solid curve: base case with $Db=10$; dashed curve: $Db\text{-base}=10$ with three times the base case impeller speed; dotted curve: Newtonian liquid agitated at $Re=6 \cdot 10^3$.

Figure 1. The two stirred tank geometries considered in this paper. Top: baffled tank with Rushton turbine (left: side view, right: top view); bottom: baffled tank with pitched-blade impeller. The (r,z) coordinate system has its origins in the center at the bottom of the tank.

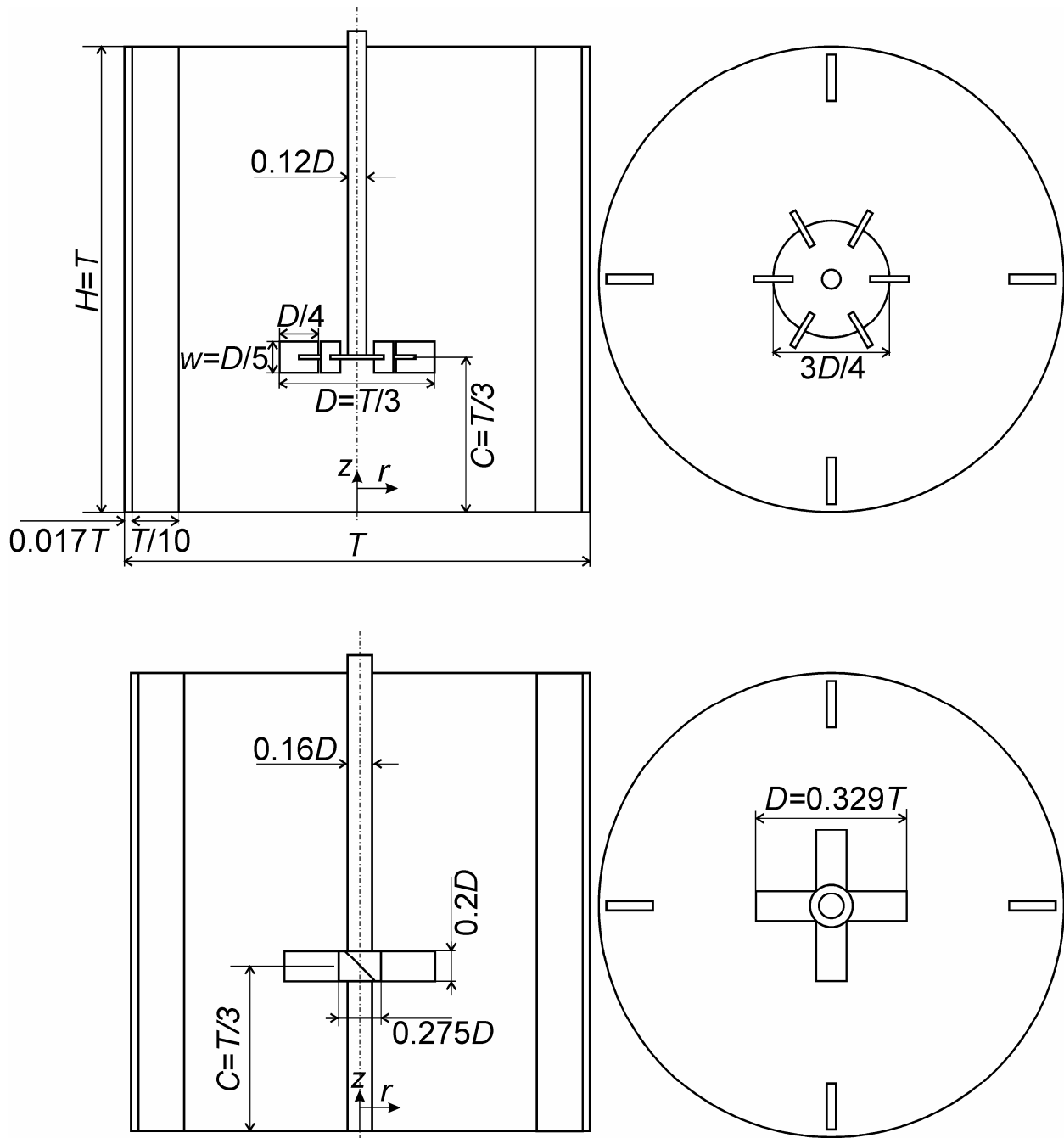


Figure 2. Steady-state rheology according to Eq. 4. The infinite-shear viscosity is η_∞ , the zero-shear viscosity is $\eta_\infty (1+\alpha)$. The pseudo yield stress τ_y is defined by extrapolating the infinite shear behavior towards $\dot{\gamma}=0$.

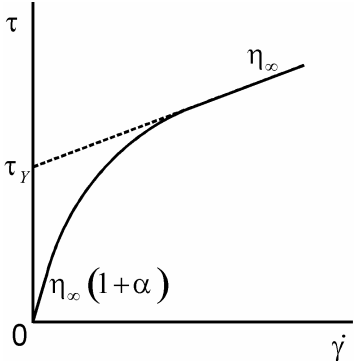


Figure 3. Time series of the tank average network parameter $\langle \lambda \rangle$ for $Db=10$, starting at $t=0$ from a zero flow field and $\lambda = 1$ everywhere. Solid line: pitched blade turbine; dashed line: Rushton turbine.

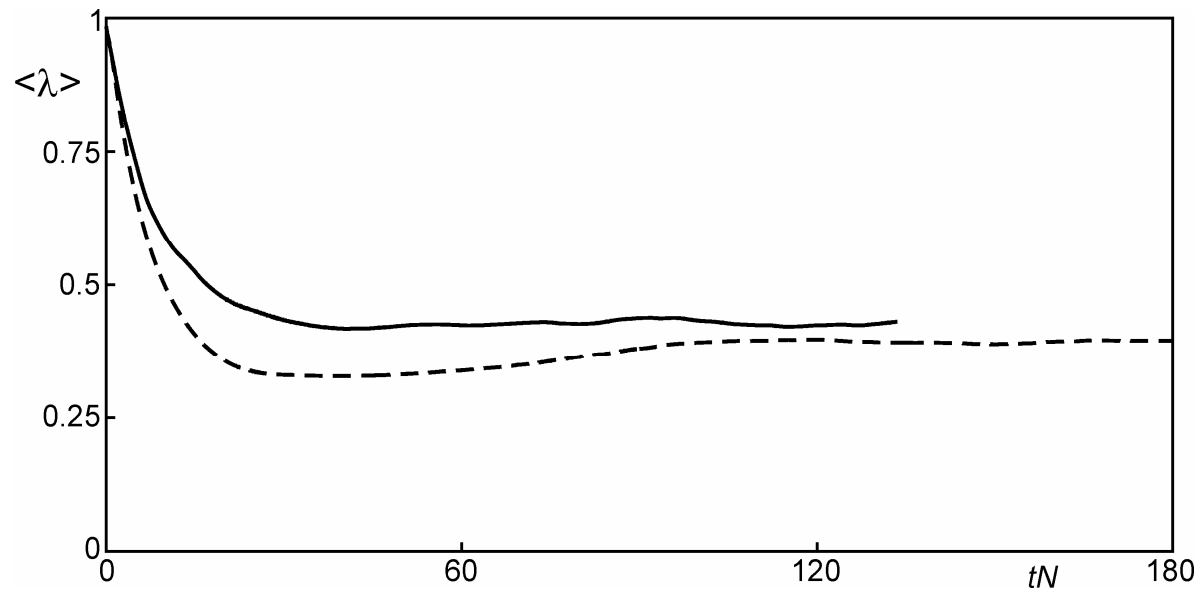


Figure 4. Instantaneous realizations of the λ -field in the vertical plane midway between baffles. Base-cases with $Db=10$. Top row: Rushton turbine flow at (from left to right) 10, 40, 70, 100, and 180 impeller revolutions after start-up; bottom row: pitched blade turbine flow after 10, 30, 90, 93, and 95 impeller revolutions.

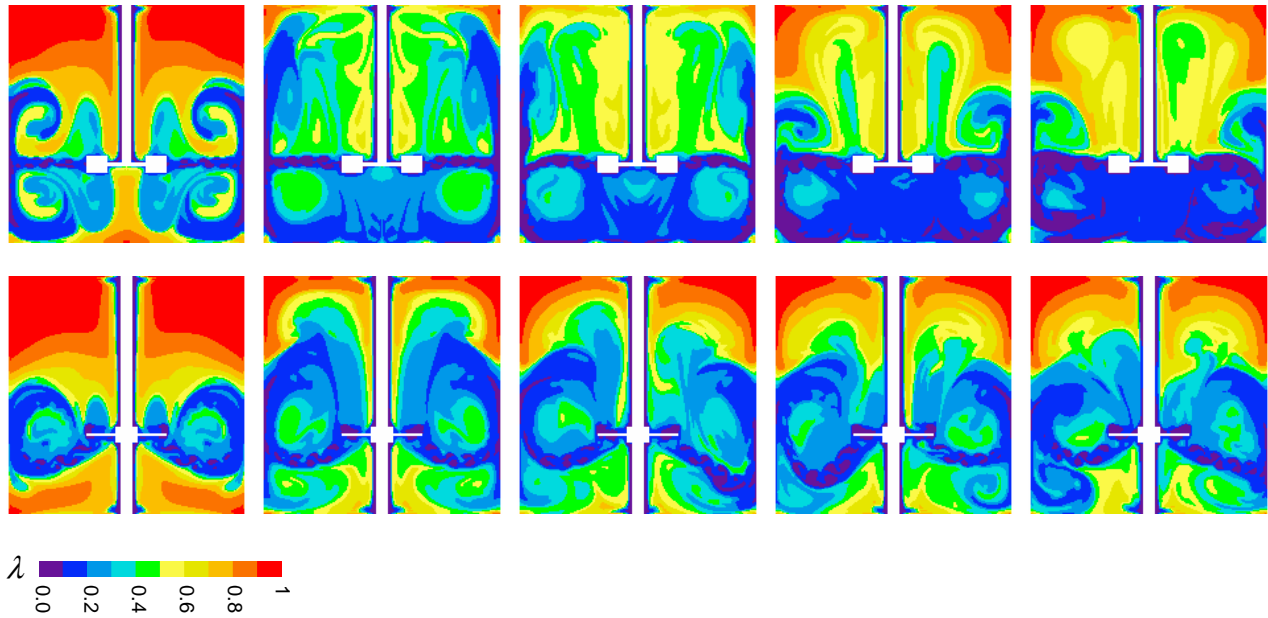


Figure 5. Time series of λ at the point $\frac{2r}{T} = 0.91, \frac{z}{T} = 0.056$ in the mid-baffle plane for the PBT case with $Db=10$.

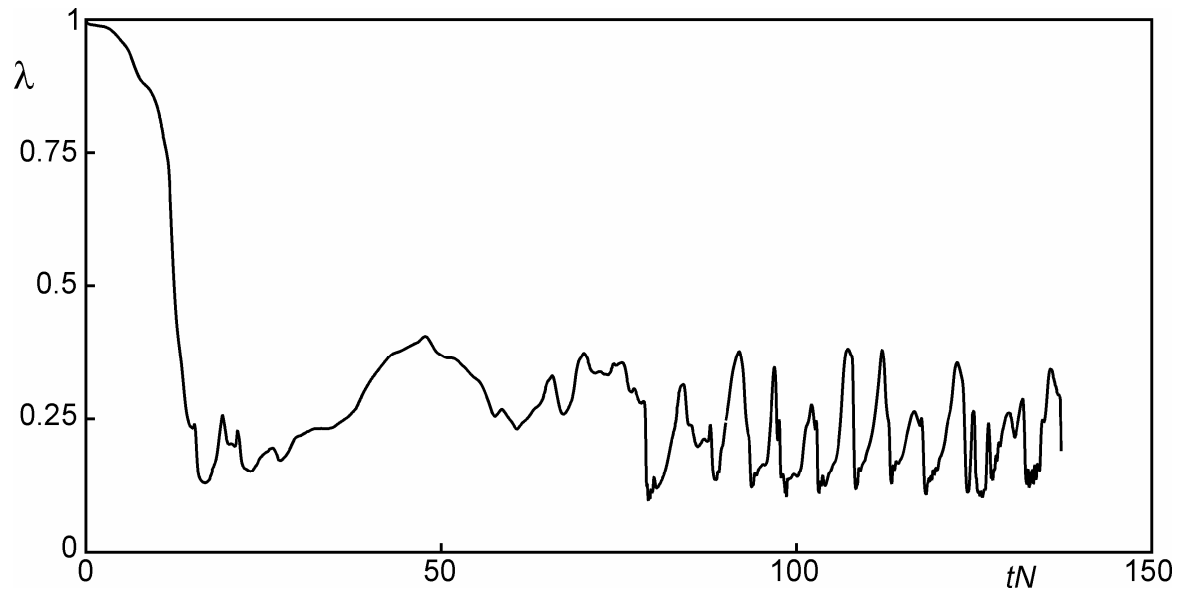


Figure 6. Time series of the tank average network parameter $\langle \lambda \rangle$ for three Deborah numbers as indicated. Top panel: pitched-blade turbine; bottom panel: Rushton turbine.

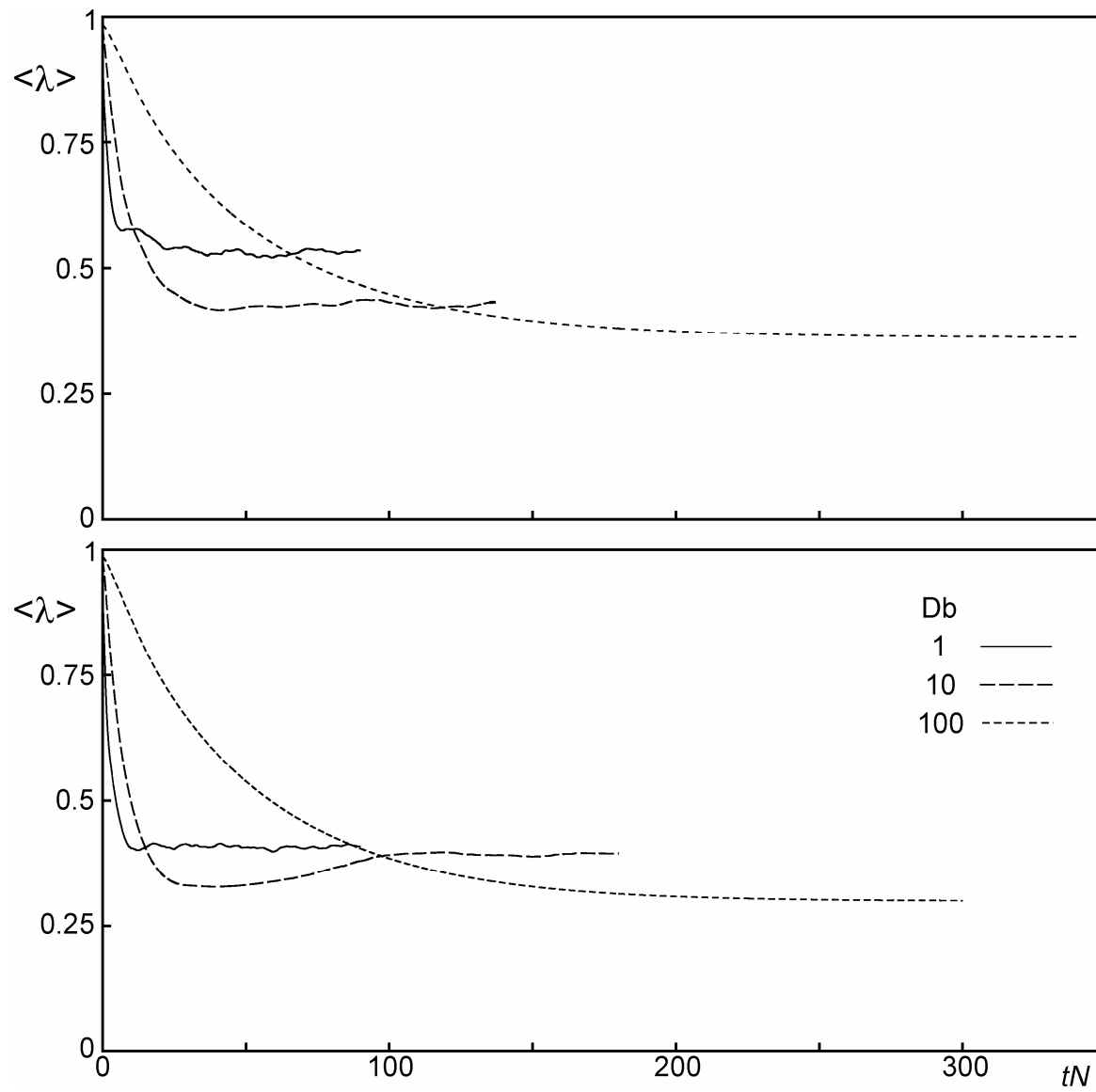


Figure 7. Instantaneous realizations of the λ -field in the vertical plane midway between baffles after quasi steady-state has been reached. Top row: pitched blade turbine flow with (from left to right) $Db=0$, 1, and 100. Bottom row: Rushton turbine flow with (from left to right) $Db=0$, 1, and 100.

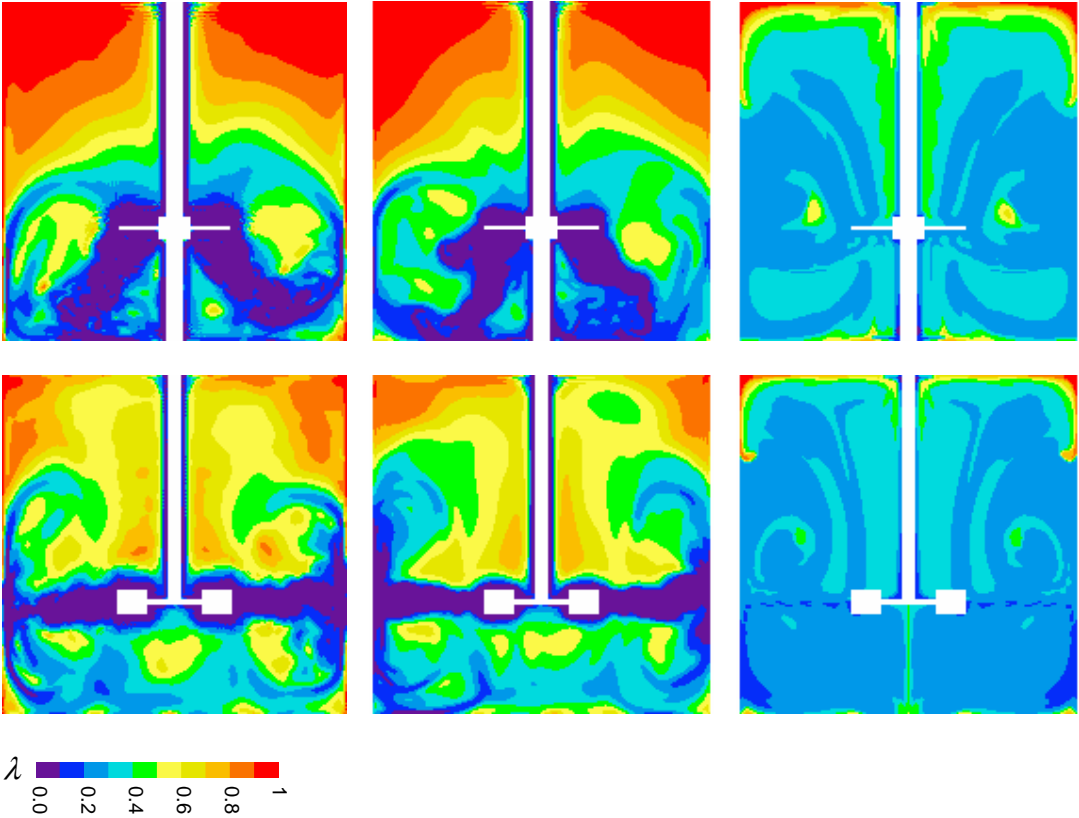


Figure 8. Snapshot of velocity vectors in the mid-baffle plane in the tank equipped with a pitched blade turbine for $Db=1$ (top-left) and $Db=100$ (top-right), and with a Rushton turbine for $Db=1$ (bottom-left) and $Db=100$ (bottom-right) after quasi steady state has been reached.

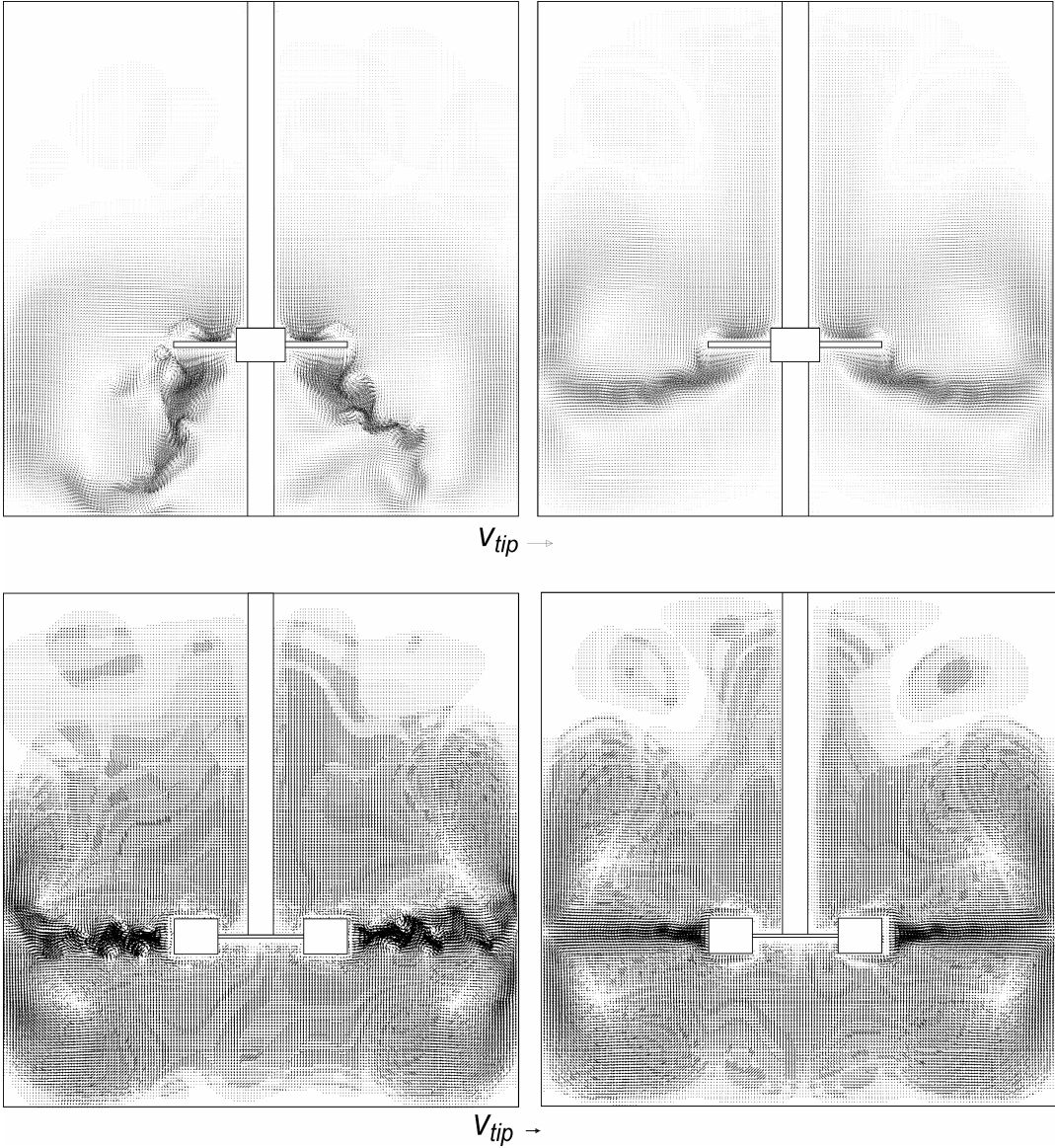


Figure 9. Time and tank-average network parameter $\overline{\langle \lambda \rangle}$ as a function of impeller speed relative to the base-case impeller speed. Time averaging was performed after (quasi) steady state was reached. The dashed line illustrates the general trend.

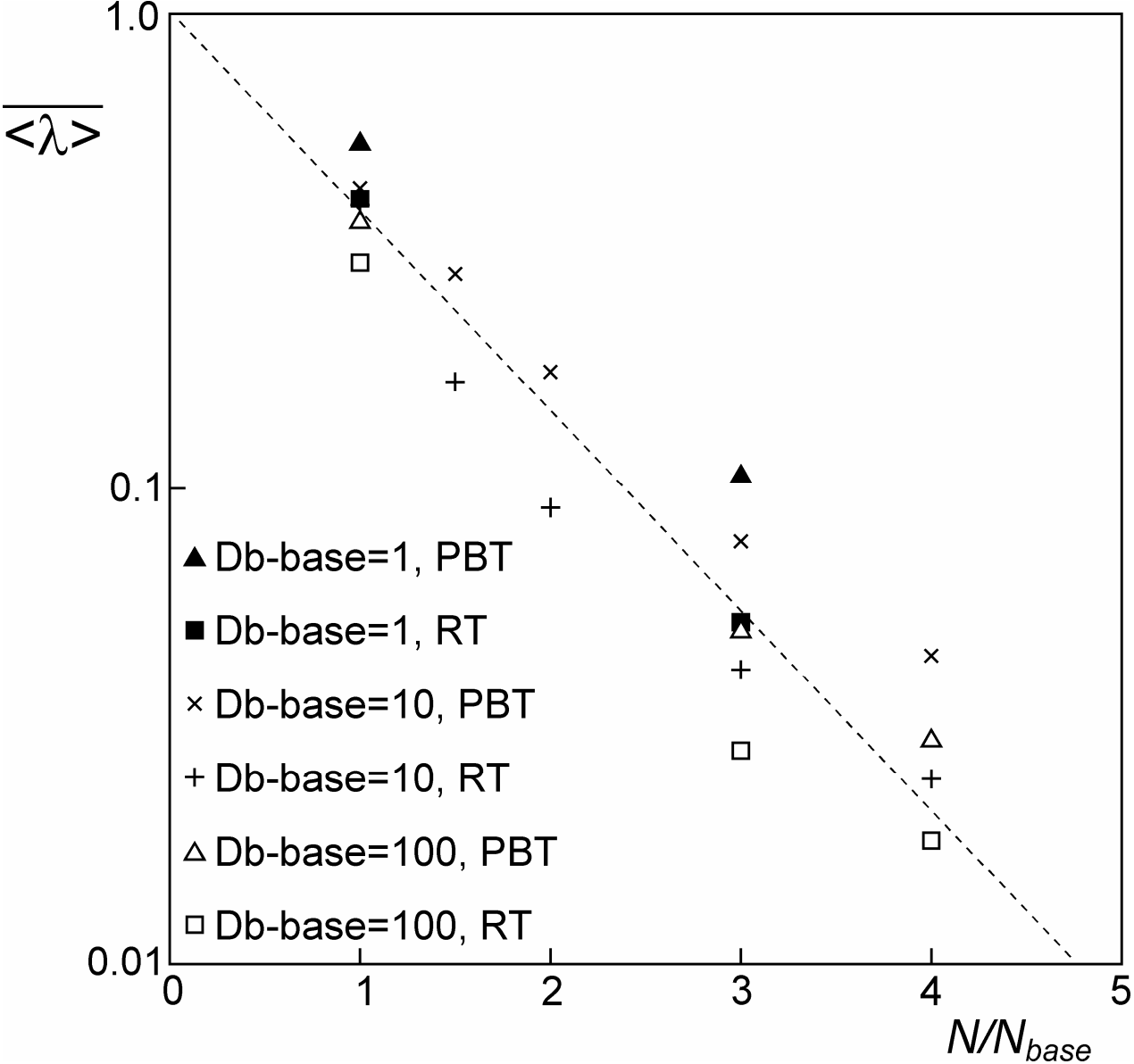


Figure 10. Snapshot of velocity vectors in a vertical, mid-baffle plane. Pitched-blade turbine flow with $Db_{-base}=1$ (left), and $Db_{-base}=100$ (right), and three times the impeller speed as the base-case.

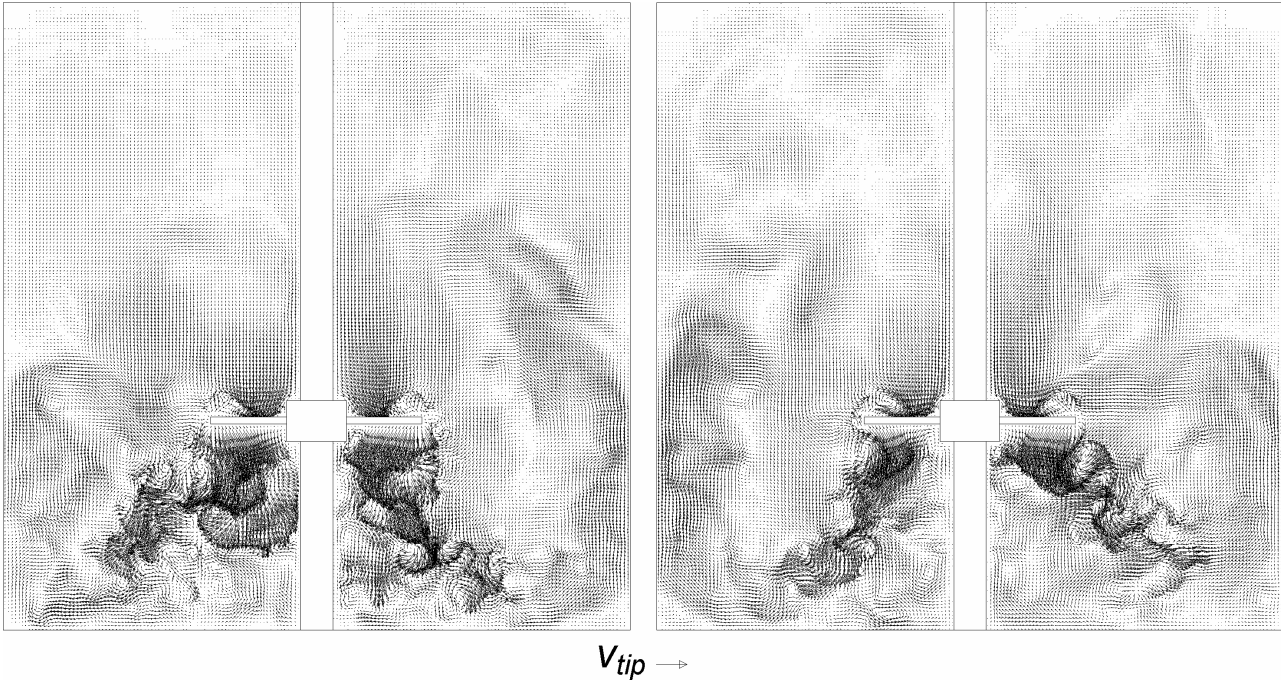


Figure 11. Snapshots of λ -contours for three times the base-case impeller speed. Pitched-blade turbine flow with (from left to right) Db -base=1, 10, 100 respectively. Note the small high- λ spots in the upper corners of the right panel.

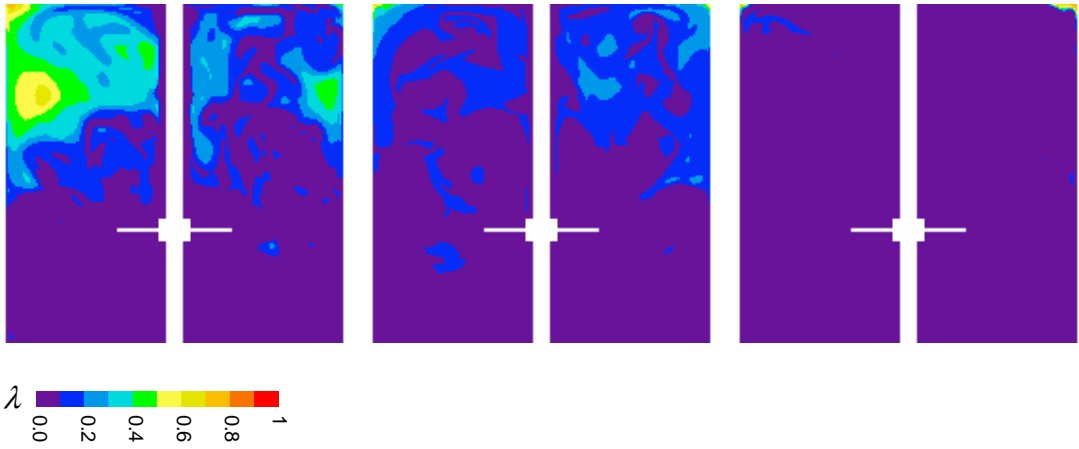


Figure 12. Time series of tank average structure $\langle \lambda \rangle$ parameter for simulations with different spatial resolution. Dashed curves: $\Delta = \frac{T}{180}$; solid curves: $\Delta = \frac{T}{240}$. Top: $Re=6000$, $Db=1$ starting from a zero flow field and $\lambda = 0$ everywhere. Bottom: $Re=18000$, $Db=30$ ($Db\text{-base}=10$) starting from a zero flow field with $\lambda = 1$ everywhere. Rushton turbine.

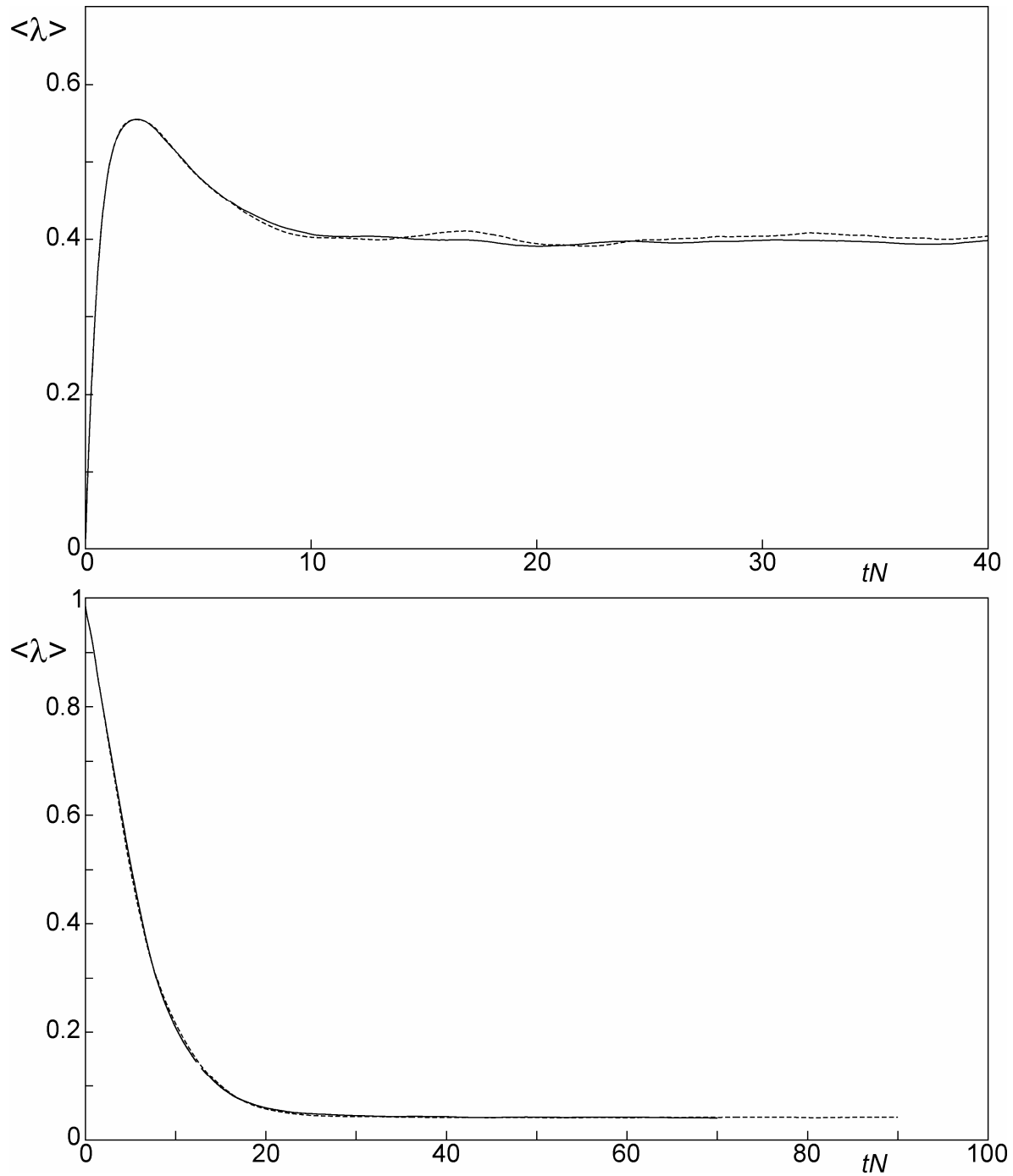


Figure 13. Averaged λ -contours in the vertical, mid-baffle plane for Rushton turbine simulations. These are impeller-angle resolved averages, i.e. the averages are conditioned with the impeller angle. In the panels shown the condition is such that an impeller blade is in the mid-baffle plane. Top row: $Re=6000$, $Db=1$; left resolution such that $\Delta = \frac{T}{180}$, right $\Delta = \frac{T}{240}$. Bottom row: $Re=18000$, $Db=30$ (Db -base=10); left resolution such that $\Delta = \frac{T}{180}$, right $\Delta = \frac{T}{240}$.

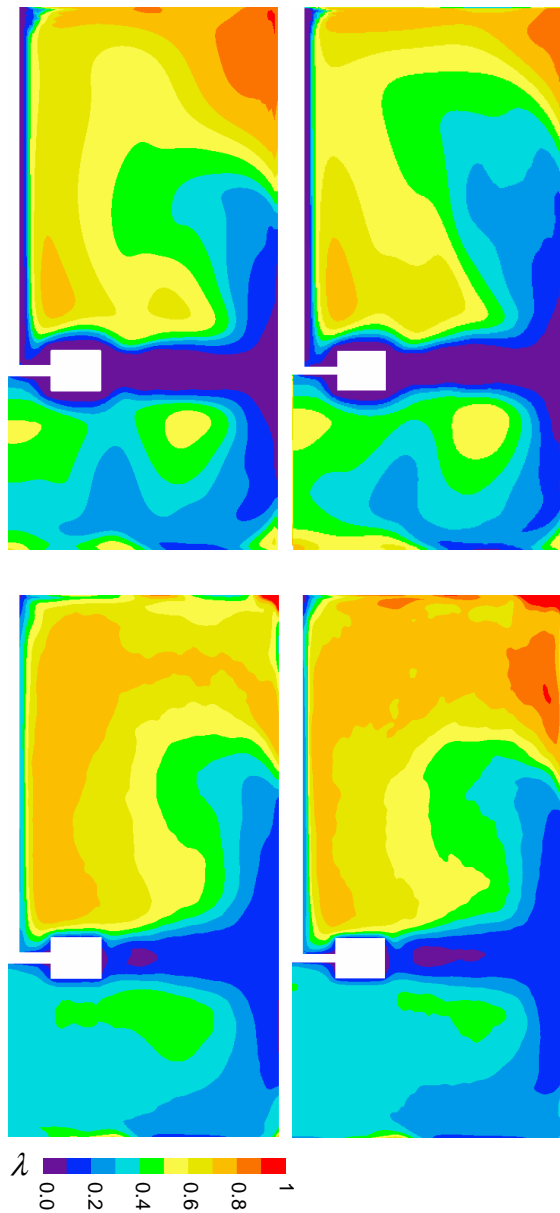


Figure 14. Instantaneous passive scalar concentrations in vertical mid-baffle planes. Left panels: 20 revolutions after start up; right panels: 40 revolutions after start up. Top: Newtonian liquid agitated at $Re=6000$; middle: base-case with $Db=10$; bottom: Db -base=10 with a 3 times higher impeller speed.

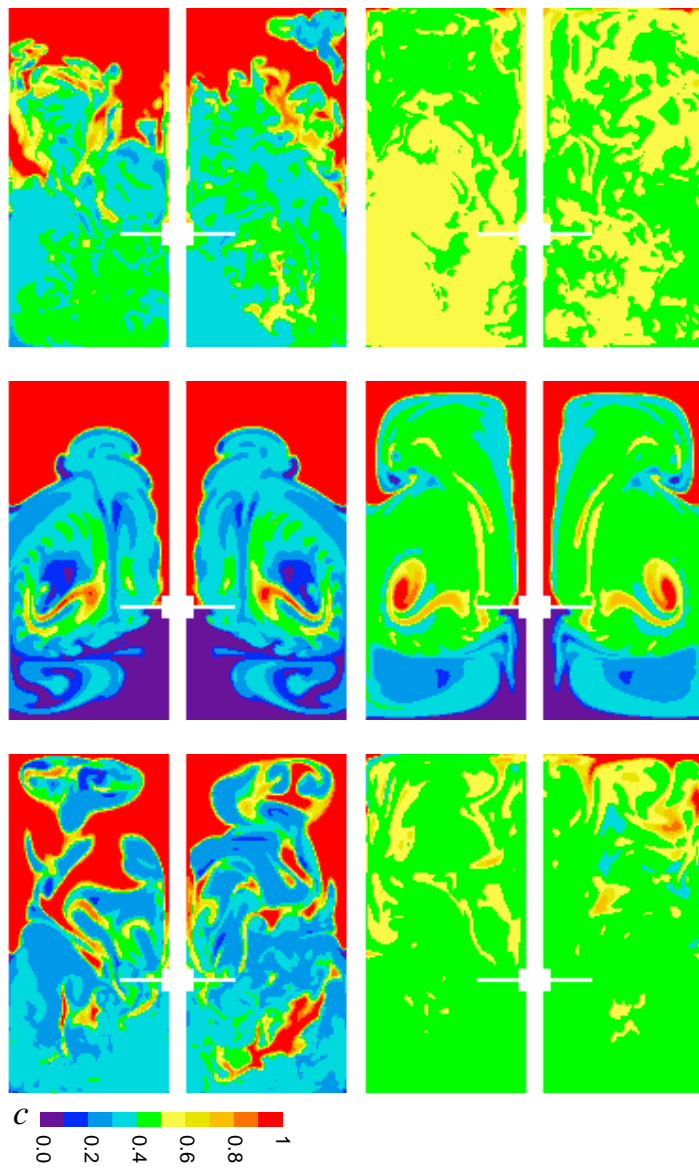


Figure 15. Time series of the passive scalar standard deviation σ in the vertical, mid-baffle plane. Solid curve: base case with $Db=10$; dashed curve: Db -base=10 with three times the base case impeller speed; dotted curve: Newtonian liquid agitated at $Re=6 \cdot 10^3$.

